

# Neutrinoless Double Beta Decay in Light of JUNO First Data

Shao-Feng Ge <sup>\*1,2</sup>, Chui-Fan Kong <sup>†3</sup>, Manfred Lindner <sup>‡4</sup>, and João Paulo Pinheiro <sup>§1,2</sup>

<sup>1</sup>State Key Laboratory of Dark Matter Physics, Tsung-Dao Lee Institute & School of Physics and Astronomy, Shanghai Jiao Tong University, Shanghai 200240, China

<sup>2</sup>Key Laboratory for Particle Astrophysics and Cosmology (MOE) & Shanghai Key Laboratory for Particle Physics and Cosmology, Shanghai Jiao Tong University, Shanghai 200240, China

<sup>3</sup>Particle Theory and Cosmology Group (PTC), Center for Theoretical Physics of the Universe (CTPU), Institute for Basic Science, Daejeon 34126, Republic of Korea

<sup>4</sup>Max-Planck-Institut für Kernphysik, Heidelberg 69117, Germany

November 20, 2025

## Abstract

The first results from the JUNO reactor neutrino oscillation experiment improve our knowledge of neutrino masses and mixing parameters, especially the solar angle  $\theta_s \equiv \theta_{12}$  and the solar mass squared difference  $\Delta m_s^2 \equiv \Delta m_{21}^2$ . We discuss the implications of these results on neutrinoless double beta decay by itself and in combination with the global fit of neutrino oscillation experiments, the JUNO first data, and cosmological constraints on the neutrino mass sum. For the effective mass  $\langle m_{ee} \rangle$ , the uncertainties in its lower limits for both mass orderings and upper limits for the normal ordering are largely reduced. Since the cosmological CMB and DESI BAO data put a stringent constraint on the neutrino mass scale, we also show how the probability distribution of both the real and imaginary parts of the effective mass  $\langle m_{ee} \rangle$  on the complex plane is affected. Especially, the funnel region with  $|\langle m_{ee} \rangle| \lesssim 1$  meV receives larger chance to happen. Correspondingly, the chance of determining the two Majorana CP phases simultaneously in this region also increases with reduced uncertainty.

---

\*[gesf@sjtu.edu.cn](mailto:gesf@sjtu.edu.cn)

†[kongcf@ibs.re.kr](mailto:kongcf@ibs.re.kr)

‡[lindner@mpi-hd.mpg.de](mailto:lindner@mpi-hd.mpg.de)

§[joaopaulo.pinheiro@fqa.ub.edu](mailto:joaopaulo.pinheiro@fqa.ub.edu)

# 1. Introduction

The baryon asymmetry of the Universe, namely that almost no anti-matter exists in Nature [1, 2], is one of the main problems in contemporary astroparticle physics and cosmology. An inflationary phase at the beginning of our Universe dilutes all pre-existing matter [3] which requires a mechanism to understand the observed baryon asymmetry. The Sakharov conditions [4] summarize the essential ingredients which must be fulfilled. One very well motivated mechanism is leptogenesis [5] which is typically related to Majorana neutrino masses with additional CP phases emerging by the seesaw mechanism [6–19].

Verifying the Majorana nature of neutrinos is therefore very important for justifying the vanilla leptogenesis mechanism. Although the ultra-violet physics at high energy is difficult to observe with current technology, with two exceptions of cosmic string [20] and cosmological collider [21], the nature inherited by light active neutrinos can manifest itself in the neutrinoless double beta decay ( $0\nu 2\beta$ ) process where a mother nuclei decays into a daughter nuclei plus two electrons,  ${}^Z_A N \rightarrow {}^Z_{A+2} N + 2e^-$  [22–25]. With two electrons appearing in the final state, such process indicates that the lepton number is violated by two. In the minimal scenario, the  $0\nu 2\beta$  decay can be induced by an effective Majorana mass  $m_{ee}$  of the light active neutrinos in the electron flavor. Reciprocally, a lepton number violating process would finally contribute to a light Majorana mass [26].

However, the  $0\nu 2\beta$  decay process involves not just particle physics, but also nuclear reaction and atomic effects. The decay half-life can be expressed as

$$(T_{1/2}^{0\nu})^{-1} \equiv G^{0\nu} |M^{0\nu}|^2 |\langle m_{ee} \rangle|^2, \quad (1.1)$$

where  $G^{0\nu}$  is the phase space factor [27–30] associated with the decay kinematics and atomic physics,  $M^{0\nu}$  is the nuclear matrix element (NME), and  $\langle m_{ee} \rangle$  is the effective electron neutrino mass from particle physics. Of these three parts, the phase space factor can be calculated very precisely while the NME suffers a lot from theoretical uncertainties [24]. The NME calculations involve complex nuclear many-body physics and depend on the nuclear structure models. There are multiple theoretical approaches such as the quasiparticle random phase approximation (QRPA) [31–35], interacting shell mode (ISM) [36–39], energy density functional methods (EDF) [40–42], interacting boson model (IBM) [43, 44], and ab initio techniques [45–51]. Their predictions typically differ by a factor of  $2 \sim 3$ , representing the main source of systematic uncertainty from the nuclear physics side [24].

On the other hand, the particle physics side has improved quite significantly. The improvement comes from neutrino oscillation experiments, beta decay spectrum measurement around the end point, and cosmology. Especially, there is complementarity between the reactor neutrino oscillation experiments and  $0\nu 2\beta$  decay [52–58] since both involves only the electron flavor and share the same set of neutrino oscillation parameters. To be exact, only two mixing angles, the reactor angle  $\theta_r \equiv \theta_{13}$  and the solar angle  $\theta_a \equiv \theta_{12}$  can appear in the effective Majorana

mass  $m_{ee}$  for  $0\nu 2\beta$  decay and the disappearance probability  $P_{ee}$  of reactor neutrino oscillation. In addition, the solar mass squared difference  $\Delta m_s^2 \equiv \Delta m_{21}^2$  and the atmospheric one  $\Delta m_a^2 \equiv \Delta m_{31}^2$  can also enter. It is interesting to see that these four oscillation parameters can be precisely measured with the combination of Daya Bay and JUNO [59, 60]. Especially, the recent global fits [61] and JUNO first data [62] have significantly reduced the uncertainty of the solar angle  $\theta_s$ . In addition, the KATRIN experiment provides the best measurement of the beta decay spectrum to put a  $\sum_i m_i \leq 0.45$  eV limit at 90% C.L. (confidence level) [63, 64]. The most stringent bound on the absolute neutrino mass comes from the recent DESI BAO data [65, 66], plus other existing observations such as CMB [67].

Concerning the recent progress in neutrino experiments and cosmology, we would like to show how these affect the prospects of the  $0\nu 2\beta$  decay. We first summarize the particle physics contribution to the  $0\nu 2\beta$  decay in Sec. 2. The following Sec. 3 studies the influence of the recent global fit and JUNO first data release in particular on the effective mass and half-life time. We further study the possibility for the effective mass  $\langle m_{ee} \rangle$  to fall into the funnel region and the prospect of determining the two Majorana CP phases simultaneously in Sec. 4. The conclusion of this paper can be found in Sec. 5.

## 2. Effective Majorana Mass for $0\nu 2\beta$ Decay

As summarized in Eq. (1.1), the half-life time  $T_{1/2}^{0\nu}$  contains three parts from atomic physics, particle physics, and nuclear physics, respectively. This section summarizes the effective mass  $\langle m_{ee} \rangle$  from the particle physics side. With  $\mathcal{O}(1)$  MeV energy release, the  $0\nu 2\beta$  process can only produce two electrons which explain why only  $\langle m_{ee} \rangle$  for the electron flavor can be probed.

The effective mass  $\langle m_{ee} \rangle$  is defined as:

$$\langle m_{ee} \rangle \equiv \sum_i m_i U_{ei}^2, \quad (2.1)$$

where  $m_i$  are the neutrino mass eigenvalues and  $U_{ei}$  are the PMNS mixing matrix elements. We follow the PMNS matrix parametrization [68],

$$U \equiv \mathcal{P} \begin{pmatrix} c_s c_r & s_s c_r & s_r e^{-i\delta_D} \\ -c_a s_s - s_a s_r c_s e^{i\delta_D} & c_a c_s - s_a s_r s_s e^{i\delta_D} & s_a c_r \\ s_a s_s - c_a s_r c_s e^{i\delta_D} & -s_a c_s - c_a s_r s_s e^{i\delta_D} & c_a c_r \end{pmatrix} \mathcal{Q}, \quad (2.2)$$

with  $\mathcal{P} \equiv \text{diag}\{e^{-i\beta_1}, e^{-i\beta_2}, e^{-i\beta_3}\}$  and  $\mathcal{Q} \equiv \text{diag}\{e^{-i\delta_{M1}/2}, e^{-i\delta_{M2}/2}, e^{-i(\delta_{M3}-\delta_D)/2}\}$ . The three phases  $\beta_i$  in  $\mathcal{P}$  are unphysical while  $\mathcal{Q}$  contains two physical Majorana phases. We set  $\delta_{M2} = 0$  but take  $\delta_{M1}$  and  $\delta_{M3}$  as the two independent physical Majorana phases. The benefit of using such parametrization is that when the lightest mass vanishes,  $m_1 = 0$  for the normal ordering (NO) case or  $m_3 = 0$  for the inverted ordering (IO), one physical Majorana CP phase would automatically disappear altogether. For convenience, we labeled the three mixing angles

according to the major type of experiments that fixes their values,  $\theta_a \equiv \theta_{23}$  for the atmospheric angle,  $\theta_r \equiv \theta_{13}$  for the reactor angle, and  $\theta_s \equiv \theta_{12}$  for the solar angle.

Note that the third element of  $\mathcal{Q}$  is defined as  $e^{-i(\delta_{M3}-\delta_D)/2}$  where the Dirac CP phase  $\delta_D$  is to cancel the same Dirac CP phase associated with the reactor angle  $s_r$  of  $U$  as defined in Eq. (2.2),

$$\langle m_{ee} \rangle = m_1 |U_{e1}|^2 e^{i\delta_{M1}} + m_2 |U_{e2}|^2 + m_3 |U_{e3}|^2 e^{i\delta_{M3}}. \quad (2.3)$$

A particularly illuminating perspective emerges when treating  $\langle m_{ee} \rangle$  as a vector sum in the complex plane which can give a geometrical view [57, 69, 70]. We can decompose it into three contributions,

$$\langle m_{ee} \rangle \equiv \vec{L}_1 + \vec{L}_2 + \vec{L}_3, \quad (2.4)$$

with each vector being defined as,

$$\vec{L}_1 \equiv m_1 |U_{e1}|^2 e^{i\delta_{M1}}, \quad \vec{L}_2 \equiv m_2 |U_{e2}|^2, \quad \vec{L}_3 \equiv m_3 |U_{e3}|^2 e^{i\delta_{M3}}. \quad (2.5)$$

With our phase convention  $\delta_{M2} = 0$ ,  $\vec{L}_2$  lies along the real axis while  $\vec{L}_1$  and  $\vec{L}_3$  rotate with the corresponding Majorana CP phases  $\delta_{M1}$  and  $\delta_{M3}$ , respectively. This geometric representation will be discussed in detail in Sec. 4, where we explore how the interplay between these vectors constrains the allowed values of  $\langle m_{ee} \rangle$ .

Using the specific parametrization of the PMNS matrix as defined in Eq. (2.2), we can write the mixing matrix elements explicitly,

$$\langle m_{ee} \rangle = c_s^2 c_r^2 m_1 e^{i\delta_{M1}} + s_s^2 c_r^2 m_2 + s_r^2 m_3 e^{i\delta_{M3}}, \quad (2.6)$$

where  $(c_\alpha, s_\alpha) \equiv (\cos \theta_\alpha, \sin \theta_\alpha)$ . Note that the atmospheric mixing angle  $\theta_a$  does not appear explicitly in  $\langle m_{ee} \rangle$ , which avoids any ambiguity related to the determination of the octant of  $\theta_a$ . The  $0\nu 2\beta$  decay shares four oscillation parameters with the reactor neutrino oscillation. Besides the reactor angle  $\theta_r$  and the solar angle  $\theta_s$ , both the solar mass squared difference  $\Delta m_s^2 \equiv m_2^2 - m_1^2$  and the atmospheric mass squared difference  $\Delta m_a^2 \equiv |\Delta m_{3\ell}^2| = |m_3^2 - m_\ell^2|$  where  $\ell = 1$  for NO ( $m_1 < m_2 < m_3$ ) and  $\ell = 2$  for IO ( $m_3 < m_1 < m_2$ ) also appear. To make the physics behind the mass squared differences more explicit, we have also adopted their labels according to the major type of observations from which their values are determined.

The behavior of  $\langle m_{ee} \rangle$  significantly depends on the ordering of the neutrino mass, with fundamentally different phenomenological implications for each scenario. The main distinction arises from the lightest mass,  $m_1$  for NO and  $m_3$  for IO. This difference has direct consequences for the allowed range of  $\langle m_{ee} \rangle$ , particularly in the limit where the lightest mass is smaller than 0.1 eV. Note that distinguishing the mass ordering is the major physics goal of the JUNO experiment [60].

For NO, we express the heavier masses ( $m_2$  and  $m_3$ ) in terms of  $m_1$  and the measured mass-squared differences,

$$\langle m_{ee} \rangle = m_1 c_s^2 c_r^2 e^{i\delta_{M1}} + \sqrt{\Delta m_s^2 + m_1^2 c_r^2 s_s^2} + \sqrt{\Delta m_a^2 + m_1^2 s_r^2} e^{i\delta_{M3}}. \quad (2.7)$$

In this case,  $\langle m_{ee} \rangle$  can vanish if the Majorana phases conspire to produce a complete destructive interference between the remaining contributions. Thus, observing  $\langle m_{ee} \rangle = 0$  would not exclude the Majorana nature of neutrinos under NO.

For IO, the masses are parametrized in terms of the lightest mass  $m_3$ :

$$\langle m_{ee} \rangle = \sqrt{m_3^2 + \Delta m_a^2 - \Delta m_s^2 c_s^2 c_r^2} e^{i\delta_{M1}} + \sqrt{m_3^2 + \Delta m_a^2 c_r^2 s_s^2 + m_3 s_r^2} e^{i\delta_{M3}}. \quad (2.8)$$

The main feature of IO is that  $\langle m_{ee} \rangle$  possesses a non-zero lower bound. This lower bound, which depends on the mixing angles and mass splitting, provides a testable prediction that can potentially discriminate between mass orderings for Majorana neutrinos. The minimum values allowed for  $\langle m_{ee} \rangle$  for IO will be explored in the next Sec. 3.

### 3. Status of $0\nu 2\beta$ Observables after JUNO Results

The interplay between the neutrino oscillation parameters and the predictions for neutrinoless double-beta decay has been extensively studied in the literature, with detailed analysis of how experimental uncertainties propagate into the allowed ranges for the effective Majorana mass  $\langle m_{ee} \rangle$  [52–56, 71]. In this section, we perform an updated analysis of [56] by incorporating the latest global fit results from neutrino oscillation experiments [61] and more crucially the first measurement of solar oscillation parameters  $\sin^2 \theta_s$  and  $\Delta m_s^2$  from the JUNO experiment [62]. Our goal is to quantify how the improved determination of the solar mixing angle  $\theta_s$  from the JUNO initial 59.1-day dataset impacts the theoretical predictions of  $\langle m_{ee} \rangle$ .

As commented in the previous Sec. 2, different neutrino mass orderings have very different phenomenological consequences on the effective  $\langle m_{ee} \rangle$  of  $0\nu 2\beta$  decay. While  $\langle m_{ee} \rangle$  could vanish for NO, it is bounded from not just above but also below for IO,

$$\langle m_{ee} \rangle_{\max}^{\text{IO}} \equiv \sqrt{m_3^2 + \Delta m_a^2 c_s^2 c_r^2} + \sqrt{m_3^2 + \Delta m_a^2 - \Delta m_s^2 s_s^2 c_r^2} + m_3 s_r^2, \quad (3.1a)$$

$$\langle m_{ee} \rangle_{\min}^{\text{IO}} \equiv \sqrt{m_3^2 + \Delta m_a^2 c_s^2 c_r^2} - \sqrt{m_3^2 + \Delta m_a^2 - \Delta m_s^2 s_s^2 c_r^2} - m_3 s_r^2. \quad (3.1b)$$

The upper and lower limits happen when the two Majorana phases take specific values to give constructive or destructive interference, respectively.

As shown in the left panel of Fig. 1, these two limits become flat when the lightest mass,  $m_1$  for NO and  $m_3$  for IO, approaches zero. More generally, a vanishing lightest mass would not have much effect on the  $0\nu 2\beta$  effective mass  $\langle m_{ee} \rangle$ . Then, only the two mixing angles ( $\theta_r$  and  $\theta_a$ ) and the two mass squared differences ( $\Delta m_a^2$  and  $\Delta m_s^2$ ) enters. For IO,

$$\langle m_{ee} \rangle_{\max}^{\text{IO}} \approx \sqrt{\Delta m_a^2} c_r^2, \quad \langle m_{ee} \rangle_{\min}^{\text{IO}} \approx \sqrt{\Delta m_a^2} (c_s^2 - s_s^2) c_r^2. \quad (3.2)$$

Although both mass squared differences are involved in the electron flavor effective mass  $\langle m_{ee} \rangle$ , the limits are dominated by the atmospheric one  $\Delta m_a^2$  with much larger value. Further, the upper limit  $\langle m_{ee} \rangle_{\max}^{\text{IO}}$  even becomes independent of the solar angle  $\theta_s$ . Since both the atmospheric

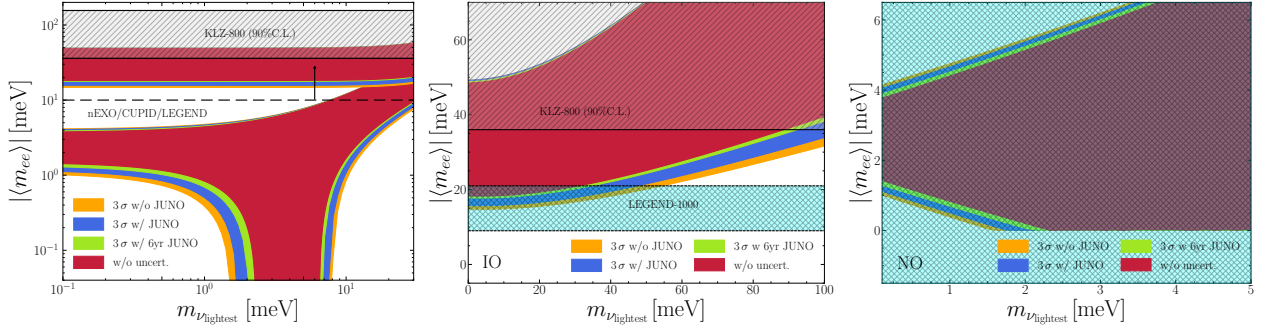


Fig. 1: The particle physics uncertainties for the  $0\nu 2\beta$  decay effective mass  $\langle m_{ee} \rangle$ . For comparison and easy viewing, three panels are shown: **(Left)** overall features for both NO and IO; **(Middle)** zoomed-in linear plot for IO; **(Right)** zoomed-in linear plot of the low-mass horizontal branch for NO. The allowed regions of the effective mass  $\langle m_{ee} \rangle$  have been demonstrated with four different uncertainty configurations: **(1)** the current  $3\sigma$  range from NuFIT 6.0 global fit (orange); **(2)** the updated  $3\sigma$  range with the JUNO first data release (blue); **(3)** the expected  $3\sigma$  range with full JUNO (green); **(4)** the ultimate scenario with negligible uncertainty (red). The current best limit on the effective mass  $\langle m_{ee} \rangle$  from KamLAND-Zen with 800 kg Xenon mass has been added as hashed region with solid boundaries while the expected sensitivities from CUPID, LEGEND1000 and nEXO are shown in the left plot as dashed line without uncertainties of nuclear matrix elements. The middle plot includes the sensitivity of LEGEND1000 including uncertainties of nuclear matrix elements.

mass squared difference  $\Delta m_a^2$  and the reactor angle  $\theta_r$  have been measured quite precisely with just roughly 1% error [61], there is almost no uncertainty in the upper limit for IO. This has been clearly shown in Fig. 1 as the filled regions for IO have roughly the same upper boundary.

For comparison, the lower limit  $\langle m_{ee} \rangle_{\min}^{\text{IO}}$  depends on not just  $\Delta m_a^2$  and the reactor angle  $\theta_r$  but also the solar angle  $\theta_s$ . Although  $\theta_s$  has also been measured very precisely with only 2% uncertainty [61], the combination  $\cos 2\theta_s$  that appears in  $\langle m_{ee} \rangle_{\min}^{\text{IO}}$  can vary by 1/3 within the  $3\sigma$  range. Even in the left panel of Fig. 1 with logarithmic scale, the effect of improving the solar angle measurement with JUNO can be clearly seen. Since the lower limit  $\langle m_{ee} \rangle_{\min}^{\text{IO}}$  corresponds to the maximal value of half-life time  $T_{1/2}^{0\nu}$  according to Eq. (1.1), such uncertainty would have significant consequences when interpreting the experimental data. Any improvement in the determination of  $\theta_s$  would significantly reduce the uncertainty on the lower bound of  $\langle m_{ee} \rangle$  for IO [56, 71].

For NO, the effective mass in Eq. (2.7) is also bound from below and above with a vanishing lightest mass  $m_1 \rightarrow 0$ ,

$$\langle m_{ee} \rangle_{\min}^{\text{NO}} \approx \sqrt{\Delta m_s^2 c_r^2 s_s^2} - \sqrt{\Delta m_a^2 s_r^2}, \quad \langle m_{ee} \rangle_{\max}^{\text{NO}} \approx \sqrt{\Delta m_s^2 c_r^2 s_s^2} + \sqrt{\Delta m_a^2 s_r^2}. \quad (3.3)$$

These two limits contain two mass squared differences and two mixing angles. Since the reactor angle  $\theta_r$  is not large, its cosine is roughly  $c_r \approx 1$ . The relative size between the two terms in Eq. (3.3) is then determined by comparing the ratios  $\Delta m_s^2 / \Delta m_a^2$  and  $s_r^2 / s_s^2$ . According to the global fit [61],  $\sqrt{\Delta m_s^2 / \Delta m_a^2} \approx 0.17$  and  $s_r^2 / s_s^2 \approx 0.07$  which means the first term  $\sqrt{\Delta m_s^2 c_r^2 s_s^2}$  dominates. Note that the solar angle  $s_s^2$  appears in the first term. The current  $3\sigma$  variation of  $s_s^2$  can be as large as 23% [61]. Although the solar mass squared difference  $\Delta m_s^2$  itself varies

by  $\sim 15\%$  at  $3\sigma$ , its contribution to  $\langle m_{ee} \rangle$  is only  $\sim 7.5\%$ . So  $\theta_s$  is the dominant source of uncertainty for NO. With all factors combined, the total effect of those uncertainties from the current data can be clearly seen in the orange bands of the left and right panels of Fig. 1. The difference is much more visible for the lower limits. This is because the variation in the first term  $\sqrt{\Delta m_s^2 c_r^2 s_s^2}$  actually affects the central values as well and the whole NO branch in the limit of vanishing lightest mass moves vertically. While the lower limit  $\langle m_{ee} \rangle_{\min}^{\text{NO}}$  is different between the two terms in Eq. (3.3), the upper one  $\langle m_{ee} \rangle_{\max}^{\text{NO}}$  is a sum with larger value. Then the relative variation is much smaller for the upper limit.

To make the influence of  $\theta_s$  on the effective mass  $\langle m_{ee} \rangle$  more visible, we have included two linear scale plots for IO and NO as the middle and right panels of Fig. 1. From this figure, it is also possible to infer from the orange bands both the minimum and maximum values of the effective mass for each mass ordering in the vanishing lightest mass scenario. Explicitly, their  $3\sigma$  intervals are  $\langle m_{ee} \rangle_{\min}^{\text{IO}} = (15.72 \sim 22.28) \text{ meV}$ ,  $\langle m_{ee} \rangle_{\min}^{\text{NO}} = (1.188 \sim 1.828) \text{ meV}$ , and  $\langle m_{ee} \rangle_{\max}^{\text{NO}} = (3.404 \sim 4.028) \text{ meV}$ , resulting from the propagation of the oscillation parameter uncertainties. While these uncertainties appear modest in  $\langle m_{ee} \rangle$ , their influence on the  $0\nu 2\beta$  experiments is much more significant [56]. Especially, the half-life time scales inversely with the effective mass squared,  $T_{1/2}^{0\nu} \propto 1/|\langle m_{ee} \rangle|^2$  according to Eq. (1.1). The variation in  $\langle m_{ee} \rangle$  would get amplified when propagating to the half-life time. Further, to reach the required sensitivity on  $T_{1/2}^{0\nu}$  the expected experimental exposure scales [72],  $M \times t \propto T_{1/2}^{0\nu}$  where  $M$  is the detector target mass and  $t$  is the running time, with the half-life time squared. Finally, the experimental exposure can differ by a factor of 4.3 for IO and 2.5 for NO. The improvement on the uncertainty from the particle physics side by JUNO is expected to significantly reduce the uncertainty in the experimental design and data interpretation.

Following the first data release from JUNO, which reported 59.1 days of data taking [62], the precision on the solar angle  $\theta_s$  and the solar mass splitting  $\Delta m_s^2$  has been significantly improved to  $\sin^2 \theta_s = 0.3092 \pm 0.0087$  and  $\Delta m_s^2 = (7.50 \pm 0.12) \times 10^{-5} \text{ eV}^2$ . This corresponds to a reduction of uncertainty by approximately a factor of 0.741 at  $3\sigma$  than the global fit results from NuFIT 6.0 [61]. According to Eq. (3.2), this translates to around 22% reduction in the uncertainty of  $\langle m_{ee} \rangle_{\min}^{\text{IO}} \propto c_s^2 - s_s^2$  at  $3\sigma$ . This improvement was achieved through JUNO's unique capability to observe the low-frequency mode of the reactor antineutrino oscillation [59],

$$P_{ee} \approx 1 - c_r^4 (c_s^2 - s_s^2) \sin^2 \left( \frac{\Delta m_s^2 L}{4E_\nu} \right). \quad (3.4)$$

For simplicity, we have omitted those high-frequency mode modulated by  $\Delta m_a^2$  which are important for the mass ordering measurement. The amplitude of the low-frequency mode is approximately  $c_s^2 - s_s^2$  which is exactly the one that appears in the lower limit  $\langle m_{ee} \rangle_{\min}^{\text{IO}}$  for IO. With large statistics at JUNO, the solar angle can be measured with very high precision. At the same time, the mode frequency or equivalently the solar mass squared difference  $\Delta m_s^2$  can also be measured with comparable precision. This impressive result within just 59.1 days of data taking demonstrates JUNO's potential to achieve sub-percent precision on solar parameters

with the full dataset, making it the leading experiment for solar mixing angle determination in the coming years.

The improved determination of  $\theta_s$  and  $\Delta m_s^2$  directly translates into enhanced constraints on the effective Majorana mass  $\langle m_{ee} \rangle$ , as shown in Fig. 1. It narrows the allowed band for  $\langle m_{ee} \rangle$  in both mass orderings. Particularly, the lower bound  $\langle m_{ee} \rangle_{\min}^{\text{IO}}$  is most relevant for the sensitivity goals of next-generation  $0\nu 2\beta$  experiments.

For comparison, Fig. 1 shows four uncertainty scenarios. First, the theoretical prediction with perfect knowledge of oscillation parameters (red) that represents the ultimate goal of mitigating the uncertainty from the particle physics side to a negligible extend [56]. Second, the current  $3\sigma$  range with the pre-JUNO global fits (orange) that shows what other experiments have achieved altogether [61]. Between these two cases, there is a huge space which is exactly the existing uncertainty from particle physics. In the middle, we have show two uncertainty scenario from the JUNO experiment. The blue band shows the reduced uncertainty with the JUNO first data release [62]. The comparison between the orange (pre-JUNO) and blue (post-JUNO) bands clearly illustrates the impact of the improved solar angle measurement by JUNO with a noticeable reduction in the width of the allowed regions for both mass orderings. The green one corresponds to the expected sensitivity with 6 years of data collection [60].

From Fig. 1, it is possible to observe that the JUNO determination of  $\theta_s$  sharpens the lower edge of the IO band (compare blue vs. orange), with total uncertainty in  $\langle m_{ee} \rangle_{\min}^{\text{IO}}$  at the  $3\sigma$  C.L. by:

$$\langle m_{ee} \rangle_{\min}^{\text{IO}} = (16.36 \sim 21.48) \text{ meV}. \quad (3.5)$$

For comparison, we have also shown those expected sensitivities from  $0\nu 2\beta$  decay experiments as horizontal lines. The most stringent current bounds come from KamLAND-Zen ( $^{136}\text{Xe}$ ), yielding  $T_{1/2}^{0\nu} > 2.3 \times 10^{26}$  yr at 90% C.L., which translates to  $\langle m_{ee} \rangle < (36 \sim 156)$  meV depending on the nuclear matrix elements (NME) [73, 74]. This bound is indicated as the hashed region with solid boundaries in the left and middle panels of Fig. 1. The current experiments are beginning to probe the IO parameter space, particularly in the region where  $m_{\text{lightest}} \gtrsim 10$  meV. The next-generation  $0\nu\beta\beta$  experiments, including nEXO [75, 76], LEGEND-1000 [77, 78], and CUPID [79, 80], are projected to reach sensitivities of  $\langle m_{ee} \rangle < (5 \sim 12)$  meV, which would fully cover the IO prediction band and begin to probe the NO region.

To make the influence of the JUNO first data [62] on the  $0\nu 2\beta$  effective mass limits more explicit, Fig. 2 shows the one-dimensional  $\Delta\chi^2$  profiles for  $\langle m_{ee} \rangle_{\min}^{\text{IO}}$ ,  $\langle m_{ee} \rangle_{\min}^{\text{NO}}$ , and  $\langle m_{ee} \rangle_{\max}^{\text{NO}}$  with vanishing lightest mass ( $m_{\text{lightest}} \rightarrow 0$ ). In this limit, the residual uncertainty is contributed by the oscillation parameters  $\Delta m_a^2$ ,  $\Delta m_s^2$ ,  $\theta_s$ , and  $\theta_r$ , as discussed before. The gray dashed horizontal lines indicate the  $1\sigma$ ,  $2\sigma$ , and  $3\sigma$  confidence levels ( $\Delta\chi^2 = 1, 4, \text{ and } 9$ , respectively). For comparison, the blue curves represent the NuFIT 6.0 global fit of neutrino oscillation experiments [61] while the red curves show the improvement from the JUNO first

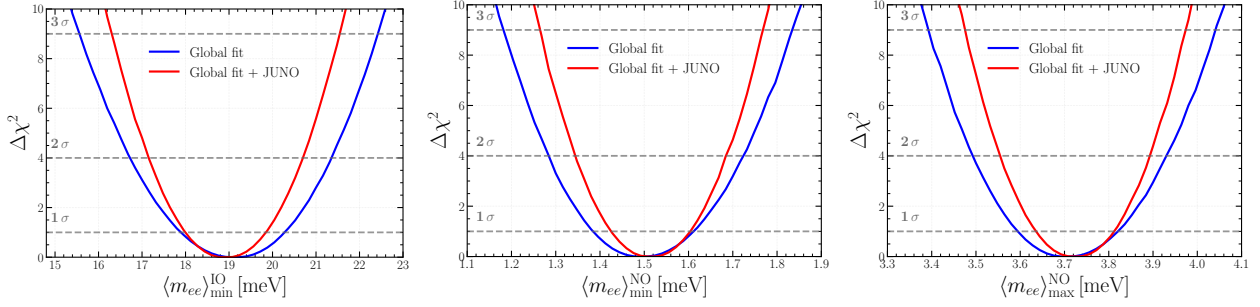


Fig. 2: One-dimensional  $\Delta\chi^2$  for the  $0\nu 2\beta$  effective mass limits  $\langle m_{ee} \rangle_{\min}^{\text{IO}}$  (left),  $\langle m_{ee} \rangle_{\min}^{\text{NO}}$  (center), and  $\langle m_{ee} \rangle_{\max}^{\text{NO}}$  (right) according to the neutrino oscillation global fit (blue) [61] or the combined results with both global fit and JUNO (red) [62].

data [62]. In all the three panels, the improvement is quite sizable which clearly shows the importance of medium baseline reactor experiments. In all three panels, the improvement is quite sizable, which clearly demonstrates the importance of medium baseline reactor experiments. Quantitatively, from the narrowing of the  $\Delta\chi^2$  profiles, one can estimate that JUNO has reduced the uncertainties on these effective mass limits by approximately 22.0% for  $\langle m_{ee} \rangle_{\min}^{\text{IO}}$ , 22.5% for  $\langle m_{ee} \rangle_{\min}^{\text{NO}}$ , and 23.1% for  $\langle m_{ee} \rangle_{\max}^{\text{NO}}$ . The corresponding  $3\sigma$  intervals after including the JUNO first data are  $\langle m_{ee} \rangle_{\min}^{\text{IO}} = (16.36, 21.48)$  meV,  $\langle m_{ee} \rangle_{\min}^{\text{NO}} = (1.268, 1.764)$  meV, and  $\langle m_{ee} \rangle_{\max}^{\text{NO}} = (3.484, 3.964)$  meV. Although JUNO does not measure the  $0\nu 2\beta$  decay directly in the first several years, it plays an important role in reducing the uncertainty from particle physics side.

Translating the measurement of the half-life time  $T_{1/2}^{0\nu}$  to the effective mass  $\langle m_{ee} \rangle$  suffers from the uncertainty in the nuclear matrix elements (NME)  $M^{0\nu}$  in Eq. (1.1). These nuclear physics uncertainties surpass those from neutrino parameter determinations. Following the framework established in [56], the Fig. 3 therein is updated as Fig. 3 with the current NME calculations extracted from [24]. Fig. 3 illustrates the current experimental limits on  $\langle m_{ee} \rangle$  versus  $T_{1/2}^{0\nu}$  for six isotopes:  $^{48}\text{Ca}$ ,  $^{76}\text{Ge}$ ,  $^{82}\text{Se}$ ,  $^{100}\text{Mo}$ ,  $^{130}\text{Te}$ , and  $^{136}\text{Xe}$ . The light blue bands indicate the nuclear uncertainties using the combined NME range of available calculations for each isotope (see Table I of [24]). Even with fixed value for the half-life time  $T_{1/2}^{0\nu}$ , there is no single fixed value of the effective mass  $\langle m_{ee} \rangle$  to be extracted.

The current experimental sensitivities on the half-life time  $T_{1/2}^{0\nu}$  at 90% C.L. are represented by the solid vertical lines in Fig. 3. Regions to the left-hand side of the vertical line have been excluded. Among various measurements, the most stringent constraints come from KamLAND-Zen ( $^{136}\text{Xe}$ ) with  $T_{1/2}^{0\nu} > 2.0 \times 10^{26}$  yr [73, 74, 81] and GERDA ( $^{76}\text{Ge}$ ) with  $T_{1/2}^{0\nu} > 1.2 \times 10^{26}$  yr [82]. Other competitive bounds include MAJORANA DEMONSTRATOR ( $^{76}\text{Ge}$ ,  $T_{1/2}^{0\nu} > 3.9 \times 10^{25}$  yr) [83], EXO-200 ( $^{136}\text{Xe}$ ,  $T_{1/2}^{0\nu} > 2.4 \times 10^{25}$  yr) [84], CUORE ( $^{130}\text{Te}$ ,  $T_{1/2}^{0\nu} > 4.8 \times 10^{25}$  yr) [85], CUPID-Mo ( $^{100}\text{Mo}$ ,  $T_{1/2}^{0\nu} > 9.7 \times 10^{24}$  yr) [86], and CUPID-0 ( $^{82}\text{Se}$ ,  $T_{1/2}^{0\nu} > 4.4 \times 10^{24}$  yr) [86].

Comparing these experimental limits with the horizontal bands in Fig. 3, we observe that the

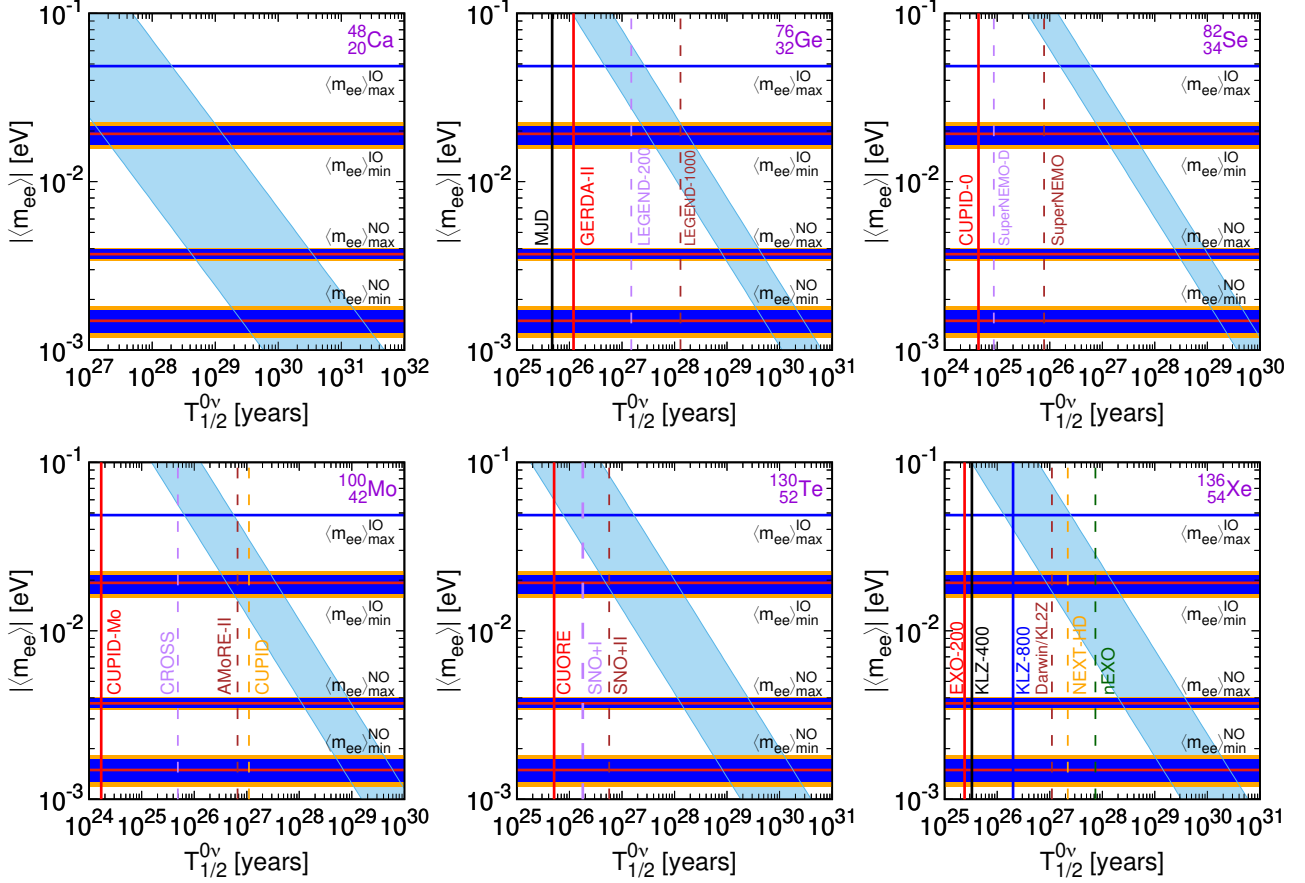


Fig. 3: The  $0\nu 2\beta$  decay half-life time  $T_{1/2}^{0\nu}$  and effective Majorana mass  $|\langle m_{ee} \rangle|$  as well as their uncertainties from the nuclear and particle physics sides. Different panels are for different isotopes. The light-blue band indicates the nuclear physics uncertainty when translating the measured half-life  $T_{1/2}^{0\nu}$  into a sensitivity on the  $0\nu 2\beta$  effective mass  $|\langle m_{ee} \rangle|$ . Current experimental limits on  $T_{1/2}^{0\nu}$  (90% C.L.) are shown as solid vertical lines with the region to the left of each solid line is excluded while the future projections are shown as vertical dashed lines. The horizontal bands show the effective mass limits for the vanishing lightest neutrino mass ( $m_{\text{lightest}} \rightarrow 0$ ):  $\langle m_{ee} \rangle_{\text{min}}^{\text{IO}}$ ,  $\langle m_{ee} \rangle_{\text{min}}^{\text{NO}}$ , and  $\langle m_{ee} \rangle_{\text{max}}^{\text{NO}}$ , with central values indicated by the red solid lines. For comparison, the orange band shows the  $3\sigma$  ranges from the current global fit while the blue band is for the combined result of global fit plus JUNO.

current experiments are beginning to probe the IO parameter space, approaching the lower edge of  $\langle m_{ee} \rangle_{\text{min}}^{\text{IO}}$ . However, they remain several orders of magnitude away from the NO region that extends from  $\langle m_{ee} \rangle_{\text{min}}^{\text{NO}}$  to  $\langle m_{ee} \rangle_{\text{max}}^{\text{NO}}$ , in the limit of vanishing lightest neutrino mass ( $m_{\text{lightest}} \rightarrow 0$ ). The orange and blue bands represent the oscillation parameter uncertainties for each of these predictions, showing how the JUNO measurement (blue band) narrows the allowed ranges compared to current global fit alone (orange band). For NO, the situation is more challenging. The maximum allowed value  $\langle m_{ee} \rangle_{\text{max}}^{\text{NO}}$  might be accessible to the next-generation experiments while the minimum value  $\langle m_{ee} \rangle_{\text{min}}^{\text{NO}}$  lies at much lower masses, requiring significantly better sensitivities than currently projected.

The effort for next-generation experiments promises a qualitative leap in sensitivity, represented by the dashed vertical lines in Fig. 3, with the flagship experiments nEXO ( $^{136}\text{Xe}$ ) [75,76] and LEGEND-1000 ( $^{76}\text{Ge}$ ) [77]. Both are projected to reach an unprecedented half-life sensitivity of  $T_{1/2}^{0\nu} \sim 10^{28}$  yr. As illustrated by the intersection of their dashed vertical lines with the light blue NME uncertainty band, the corresponding  $\langle m_{ee} \rangle$  sensitivity ranges are (6 ~ 27) meV for nEXO and (9 ~ 21) meV for LEGEND-1000. In addition, the CUPID experiment [79,80] targeting  $^{100}\text{Mo}$  and  $^{82}\text{Se}$  aims for  $T_{1/2}^{0\nu} \sim 10^{27}$  yr which can translate to  $\langle m_{ee} \rangle = (12 \sim 34)$  meV. We also include in Fig. 3 the projected sensitivities of DARWIN [87], KamLAND-Zen [88], NEXT-HD [89], SNO+ [90], AMoRE-II [91], SuperNEMO [92], and LEGEND-200 [77].

While these next-generation experiments represent impressive technical achievements, their projected sensitivities would only begin to probe the IO region near  $\langle m_{ee} \rangle_{\min}^{\text{IO}}$ , assuming favorable NME calculations. Definitive exclusion of IO would require reduction of the NME uncertainties or further experimental improvements beyond the current projections. For the NO case, these upcoming experiments remain far from accessing most of the allowed parameter space. Even with optimistic assumptions, nEXO and LEGEND-1000 would only marginally reach  $\langle m_{ee} \rangle_{\max}^{\text{NO}}$ , while the region near  $\langle m_{ee} \rangle_{\min}^{\text{NO}}$  would remain inaccessible. This highlights the critical importance of reducing the oscillation parameter uncertainties through future measurements. The combination of improved  $0\nu 2\beta$  sensitivity and precise oscillation data with reactor neutrino experiments, particularly from JUNO, will be essential for meaningful constraints on the effective mass and the neutrino mass ordering.

## 4. JUNO Impact on Majorana Triangle and Majorana CP Phases

The particle physics contribution to the  $0\nu 2\beta$  decay effective mass  $\langle m_{ee} \rangle$  is not just the two mixing angles ( $\theta_r$  and  $\theta_s$ ) and the two mass squared differences. There are two Majorana CP phases  $\delta_{M1}$  and  $\delta_{M3}$  which also come from the particle physics side. Not to say the lightest neutrino mass or the absolute mass scale. However, the neutrino oscillation experiments cannot measure neither of them. While the neutrino mass scale can be probed by the beta decay spectrum experiment KATRIN and the cosmological observations as summarized in Sec. 4.1, the only chance for measuring the two Majorana CP phases comes from the  $0\nu 2\beta$  decay itself. We will investigate how the improved oscillation parameter measurements affect the prospect of measuring the two Majorana CP phases through the Majorana triangle in Sec. 4.2.

### 4.1. Cosmological Measurement of Neutrino Mass Scale and Preference for NO

The cosmological constraints on the neutrino mass sum  $\sum_i m_i$  provide complementary information to laboratory searches. Especially, the DESI BAO measurements with CMB data gives the most stringent current bound,  $\sum_i m_i < 0.082$  eV at 95% C.L. [65,66]. For reference, the

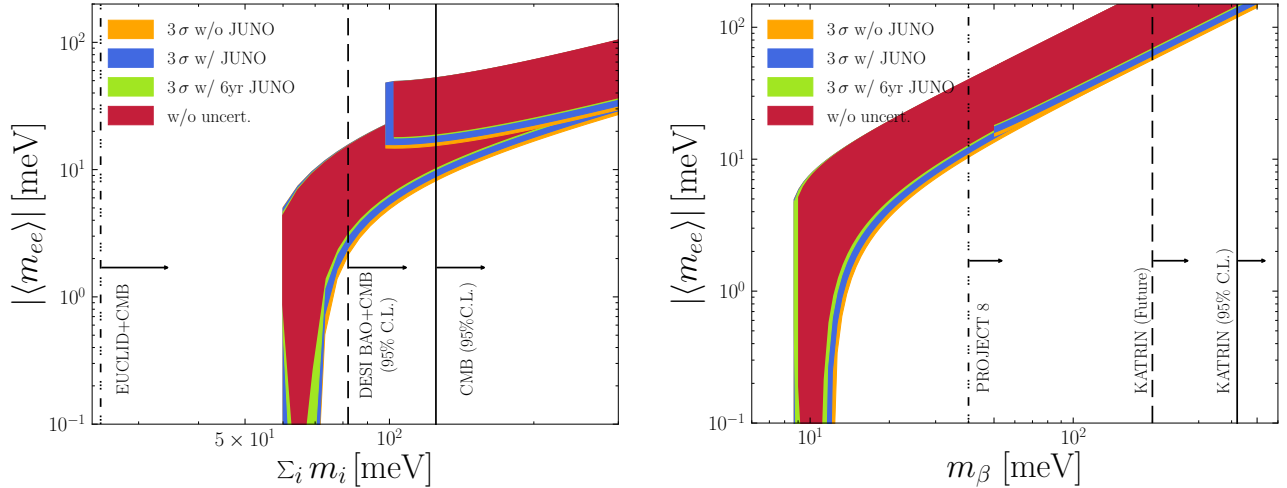


Fig. 4: **(Left)** Cosmological constraints on the neutrino mass sum  $\sum_i m_i$  at 95% C.L. with vertical line for the exiting observations from CMB (solid) and DESI BAO (dashed). For comparison, the projected sensitivities at the future EUCLID is shown as dash-dotted line. **(Right)** The current KATRIN (solid) and its design (dashed) sensitivities on the beta decay effective mass  $m_\beta$ . For comparison, the expected PROJECT 8 sensitivity is also shown as a vertical dash-dotted line. The uncertainties of the effective Majorana mass  $\langle m_{ee} \rangle$  from the particle physics side are also shown according to the the color scheme of Fig. 1.

combination of CMB data from Planck, the non-DESI Baryon Acoustic Oscillations (BAO) observation, Cosmic Chronometers (CC), and Pantheon, yields  $\sum_i m_i < 0.12$  eV at 95% C.L. [67]. These bounds are indicated in the left panel of Fig. 4 with vertical lines. The current cosmological observations have already went beyond the IO regime to probe its NO counterpart. The future cosmological surveys, such as EUCLID, are expected to reach the sensitivity of  $\sum_i m_i < 0.056$  eV [93, 94] which would directly test the global lower limit of the neutrino mass sum.

However, the cosmological measurement highly depends on the data set adopted in the analysis and the theoretical assumptions or systematics. When systematic uncertainties in the determination of cosmological parameters such as  $\sigma_8$  and  $S_8$  are properly accounted for [95–97], or when extended cosmological models such as the time-varying dark energy [98], dark matter-dark radiation interactions [99], massive neutrino self-interactions [100, 101], or other beyond  $\Lambda$ CDM scenarios [102] are considered, the constraints can be relaxed to  $\sum_i m_i \lesssim (0.1 \sim 0.15)$  eV, where the IO regime is still allowed. Besides the conventional CMB and matter power spectrum with linear dependence  $\sum_i m_i$ , the cosmic gravitational focusing with fourth power dependence  $\sum_i m_i^4$  can provide an independent cosmological measurement of the neutrino masses [103] and mass ordering [104].

The kinematic constraint  $m_\beta < 0.45$  eV at 90% C.L. [63, 64] on the beta decay effective mass  $m_\beta \equiv \sqrt{\sum_i |U_{ei}|^2 m_i^2}$  from the KATRIN experiment provides a direct and model-independent measurement of the neutrino mass scale. Although the beta decay constraint is not as strong as the cosmological observation, we also show them in the right panel of Fig. 4 for comparison.

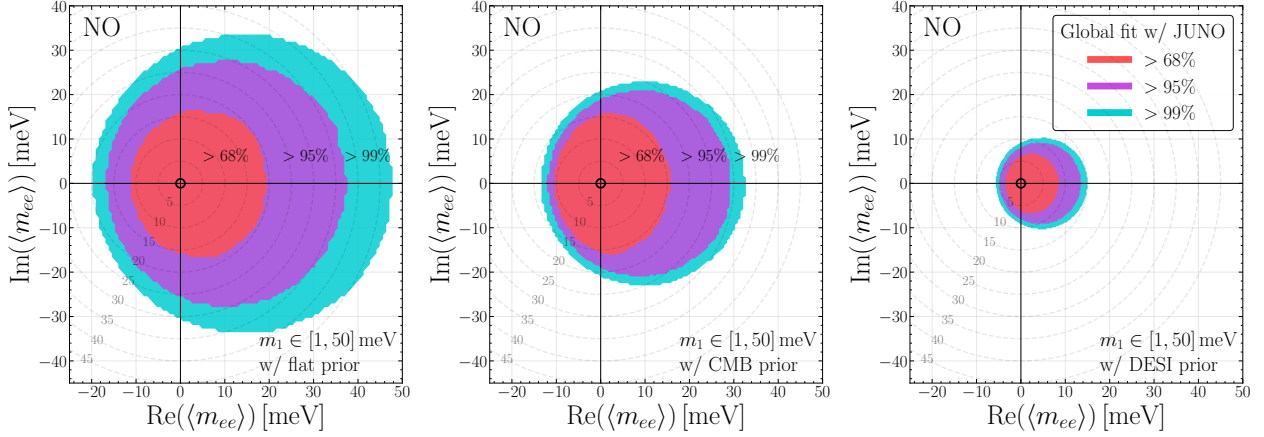


Fig. 5: Allowed regions in the complex plane of the effective mass  $\langle m_{ee} \rangle$  (real vs. imaginary parts) for NO. Three scenarios are presented: **(Left)**  $m_{\text{lightest}} \in [1, 50]$  meV with a flat prior and no cosmological bounds on  $\sum_i m_i$ ; **(Center)**  $m_{\text{lightest}} \in [1, 50]$  meV with a prior from the pre-DESI CMB cosmological bounds on  $\sum_i m_i$ ; and **(Right)**  $m_{\text{lightest}} \in [1, 50]$  meV with a prior from DESI BAO + CMB cosmological bounds on  $\sum_i m_i$ . The colored contours represent different confidence levels: red (68% C.L.), purple (95% C.L.), and cyan (99% C.L.). The black circle around the origin indicates the funnel region with  $|\langle m_{ee} \rangle| < 1$  meV.

The current laboratory measurements probe the cosmologically allowed mass range, but still remain about an order of magnitude above the sensitivity required to test the IO scenario. The KATRIN experiment is expected to reach its design sensitivity  $m_\beta \sim 0.2$  eV at 90% C.L. after several years of data taking [105]. The next-generation experiments such as PROJECT 8 are projected to reach the sensitivity of  $m_\beta \sim 0.04$  eV [106, 107], which would probe the majority of the IO regime.

As summarized in Sec. 2 and in particular Eq. (2.4), the effective mass  $\langle m_{ee} \rangle$  can be viewed as a vector sum of three contributions in the complex plane. With our phase convention  $\delta_{M2} = 0$ , the vector  $\vec{L}_2$  lies along the real axis while  $\vec{L}_1$  and  $\vec{L}_3$  rotate with the two physical Majorana CP phases  $\delta_{M1}$  and  $\delta_{M3}$ . This geometrical configuration is finally determined by the allowed ranges for  $|U_{ei}|^2$  from oscillation experiments, the relative magnitudes of the triangle sides  $L_i = m_i |U_{ei}|^2$ , and the absolute mass scale  $m_{\text{lightest}}$ .

The behavior of  $\langle m_{ee} \rangle$  in the complex plane reveals the fundamental difference between the two mass orderings. For NO, the mass hierarchy  $m_1 < m_2 \ll m_3$  allows these three vectors to form a closed triangle that can reach complete cancellation,  $\langle m_{ee} \rangle = 0$ , for specific combinations of the two Majorana CP phases [57, 69, 70]. In contrast, for IO with  $m_3 \ll m_1 < m_2$ , the relative magnitudes of the vector sides prevent such closure, making  $\langle m_{ee} \rangle = 0$  geometrically impossible regardless of the Majorana phases. Such fundamental difference manifests topologically in the complex  $\langle m_{ee} \rangle$  plane for NO.

Fig. 5 shows the allowed regions for the effective mass  $\langle m_{ee} \rangle$  with the horizontal and vertical axes denoting its real and imaginary parts, respectively. As the Majorana phases  $\delta_{M1}$  and  $\delta_{M3}$  vary over their full range  $[0, 2\pi]$ , the allowed values of  $\langle m_{ee} \rangle$  trace out a characteristic circle

region, which can be understood with the geometrical picture. The real  $L_2$  first shifts to the central point to the right. Based on this, the vector  $\vec{L}_1$  with length  $L_1 = m_1 c_s^2 c_r^2$  rotates around the shifted epicenter and the third vector  $\vec{L}_3$  with shorter length  $L_3 = m_3 s_r^2$  further scanning the whole plane. Vertically, the allowed regions are symmetric around the horizontal axis which is a manifestation of the fact that the imaginary part can flip sign when the two Majorana CP phases change their signs simultaneously.

Across the three panels of Fig. 5, the size of the circles differ considerably. The major factor is the allowed range of the neutrino mass scale. For comparison, the left panel shows the results obtained with even distribution (flat prior) of the lightest mass in the range of  $m_1 \in [1, 50]$  meV. Once the cosmological constraints are imposed in the center and right panels, the allowed circle regions shrink. The effect is not that significant for the case with only pre-DESI constraints since the limit  $\sum_i m_i < 0.12$  eV 95% C.L. [67] translates to  $m_1 \lesssim 30$  meV which is roughly the size of circle. To make the connection more direct, the corresponding upper limit for the NO effective mass in Eq. (2.8) with a nonzero  $m_1$  is,

$$\langle m_{ee} \rangle_{\max}^{\text{NO}}(m_1) = m_1 c_s^2 c_r^2 + \sqrt{\Delta m_s^2 + m_1^2 c_r^2 s_s^2} + \sqrt{\Delta m_a^2 + m_1^2 s_r^2} \approx 31 \text{ meV}. \quad (4.1)$$

However, once the DESI constraint  $\sum m_i < 0.082$  eV at 95% C.L. [65,66] is imposed, the allowed circle significantly shrinks to  $\langle m_{ee} \rangle_{\max}^{\text{NO}}(m_1) \approx 16$  meV with  $m_1 \lesssim 14$  meV.

A very important feature is that the vanishing effective mass scenario,  $\langle m_{ee} \rangle = 0$  which corresponds to the origin of the plots, is always allowed by the current constraints. This because the funnel or throat region shown in the left panel of Fig. 1 is covered by the sampling regions,  $m_1 \in [1, 50]$  meV. Even the DESI result with  $m_1 \lesssim 14$  meV still covers this funnel region as clearly indicated by the dashed line in the left panel of Fig. 4. Most importantly, the funnel region  $|\langle m_{ee} \rangle| < 1$  meV indicated by the black circle around the origin is actually in the most probable range (red band). With more stringent bound from DESI, the relative size of the funnel region with respect to the whole circle actually increases. It indicates that the chance for the  $0\nu 2\beta$  decay effective mass  $\langle m_{ee} \rangle$  to fall into the funnel region is actually increasing.

## 4.2. Determination of Two Majorana CP Phases

As shown above, the scenario of a vanishing effective mass  $\langle m_{ee} \rangle$  or being bound from above has visible chance. To focus on such scenarios, Fig. 6 shows the allowed regions in the complex  $\langle m_{ee} \rangle$  plane for NO with four representative values of the lightest mass,  $m_{\text{lightest}} = (3, 4, 5, 6)$  meV in different panels. The figure clearly illustrates the characteristic circle topology for NO that passes through the origin. For  $m_{\text{lightest}}$  in the narrow window of  $(3 \sim 6)$  meV, the 68% C.L. region (red contours) covers the origin. In other words, the three vectors can arrange themselves into a closed triangle with complete cancellation at specific combinations of  $\delta_{M1}$  and  $\delta_{M3}$  to satisfy the geometrical closure conditions. A major difference from Fig. 5 is that now the circle is not fully filled but has a black region in the middle. This is because with fixed  $m_1$ ,

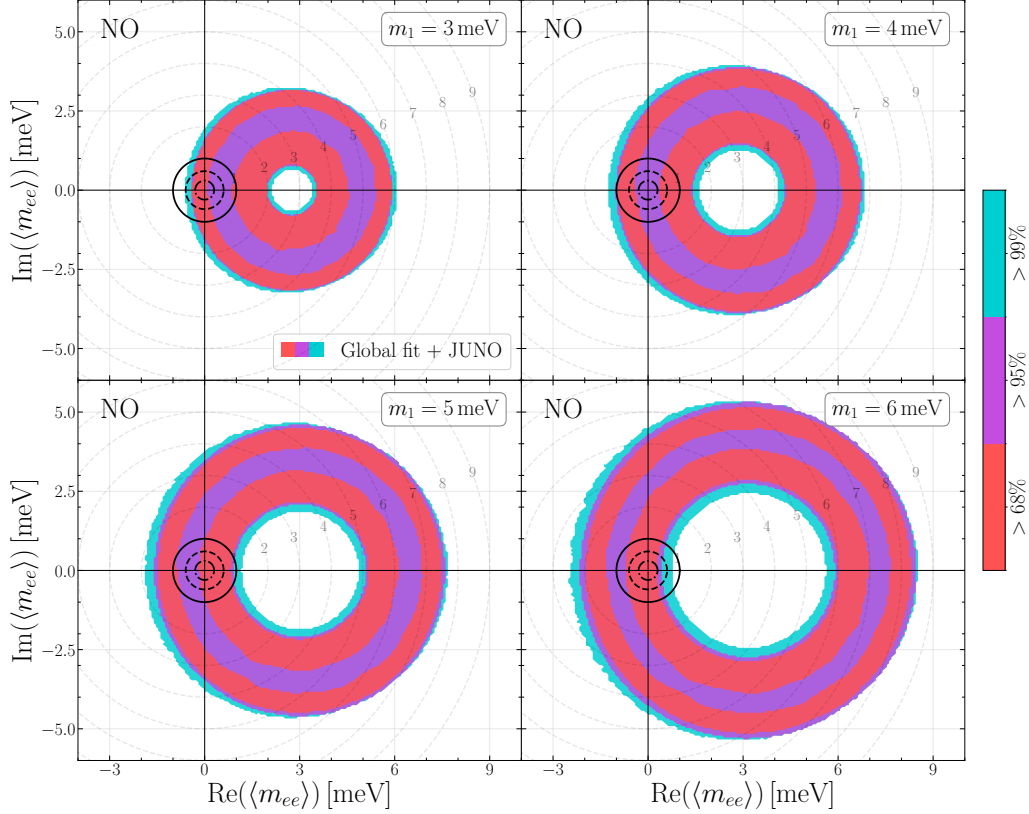


Fig. 6: Allowed regions in the complex plane of  $\langle m_{ee} \rangle$  (real vs. imaginary parts) for NO with the lightest mass  $m_1 = 3, 4, 5, 6$  meV. The filled color regions represent the 68% (red), 95% (purple), and 99% (cyan) confidence levels. The black circles indicate the funnel region with  $|\langle m_{ee} \rangle| < 1$  meV (solid), 0.6 meV (dashed), and 0.3 meV (dash-dotted).

the three vector lengths  $L_i$  cannot adjust freely, especially for  $L_2$  whose length determines the thickness of the doughnut.

If the cancellation among the three complex vectors  $\vec{L}_i$  really happens, a *Majorana triangle* can form. Then it is possible to determine the two Majorana CP phases simultaneously as function of the three vector lengths [57],

$$\cos \delta_{M1} = -\frac{L_1^2 + L_2^2 - L_3^2}{2L_1L_2}, \quad \cos \delta_{M3} = \frac{L_1^2 - L_2^2 - L_3^2}{2L_2L_3}. \quad (4.2)$$

Note that only a single degree of freedom, as a combination of the two Majorana CP phases, can be determined for a nonzero effective mass. However, a vanishing  $\langle m_{ee} \rangle$  requires both its real and imaginary parts to vanish. In other words, two independent conditions can appear in the vanishing limit to simultaneously constraint the two Majorana CP phases. This is a very rare example that one extra constraint can appear. Even if there is experimental uncertainty and hence only an upper bound on the effective mass can be extracted,  $|\langle m_{ee} \rangle| < c$ , it can transfer to both the imaginary and real parts,  $|\text{Re}(\langle m_{ee} \rangle)| < c$  and  $|\text{Im}(\langle m_{ee} \rangle)| < c$ . The funnel region has been shown with black circles with  $c = 1$  meV (solid), 0.6 meV (dashed), and 0.3 meV (dash-dotted) in Fig. 6.

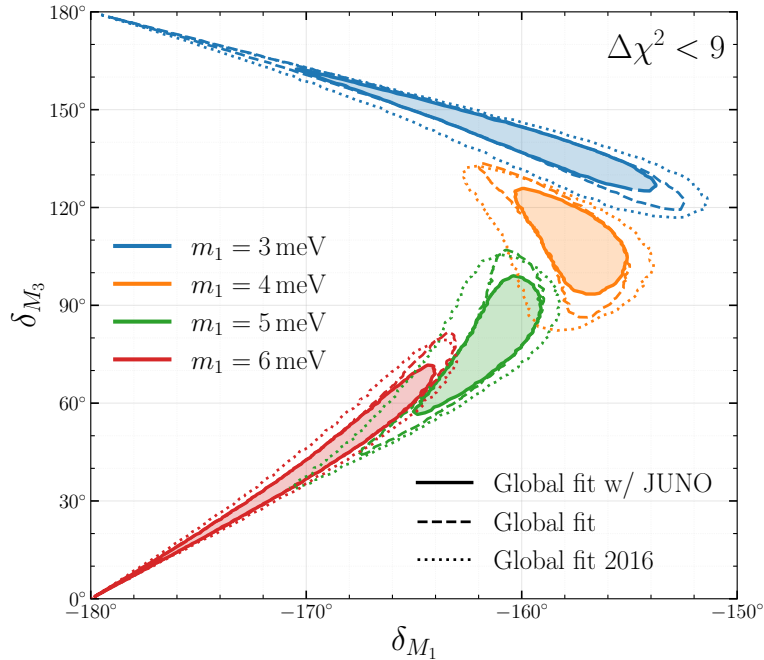


Fig. 7: The two Majorana CP phases  $(\delta_{M1}, \delta_{M3})$  determined by the Majorana triangle ( $\langle m_{ee} \rangle = 0$ ) for NO with  $m_1 = 3$  meV (blue), 4 meV (orange), 5 meV (green), and 6 meV (red). Three uncertainty schemes of the oscillation parameters with  $\Delta\chi^2 < 9$  are shown. The dotted contours represent results from the Fig. 7 of [57], dashed contours show the current NuFIT 6.0 bounds, while the thick solid contours incorporate the latest JUNO measurement.

A paradox here is that if the  $0\nu 2\beta$  decay is observed, one physical degree of freedom cannot be observed. But if the effective mass  $\langle m_{ee} \rangle$  vanishes to make the  $0\nu 2\beta$  decay invisible, both physical Majorana CP phases can be simultaneously determined. The Majorana nature can be probed with other ways, such as the direct detection of cosmic neutrino backgrounds with tritium [23, 108, 109] or the atomic radiative emission of neutrino pairs [110, 111].

Fig. 7 illustrates this possibility by showing the two Majorana CP phases  $\delta_{M1}$  and  $\delta_{M3}$  determined by the Majorana triangle ( $\langle m_{ee} \rangle = 0$ ) for NO with different values of the lightest neutrino mass  $m_1 = 3, 4, 5, 6$  meV. Each colored region represents one allowed solution: blue for 3 meV, orange for 4 meV, green for 5 meV, and red for 6 meV. These solutions are obtained by varying the oscillation parameters within  $\Delta\chi^2 < 9$  and solving Eq. (4.2) for each parameter combination. Three uncertainty schemes are displayed: the previous uncertainties used in the Fig. 7 of [57] (dotted contours), current NuFIT 6.0 bounds [61] (dashed contours), and the combination of NuFIT with the JUNO first measurement [62] (thick solid contours). The progressive narrowing of these allowed regions, particularly evident when comparing the dotted with the solid contours, directly demonstrates how the reduced uncertainties of oscillation parameters translate into more precise predictions for the Majorana phases solutions.

The comparison in Fig. 7 clearly demonstrates how the reactor experiments can help mitigating the uncertainty in  $0\nu 2\beta$  decay. The factor of  $\sqrt{2}$  reduction in the  $\theta_s$  uncertainty at JUNO

narrows the allowed region of  $\delta_{M1}$  and  $\delta_{M3}$  for each value of  $m_1$ . This reduction is particularly pronounced because  $\theta_s$  directly affects the relative magnitudes of  $L_1$  and  $L_2$  through the prefactors  $c_s^2$  and  $s_s^2$ . The narrower bands in Fig. 7 translate directly into more precise predictions. If future  $0\nu\beta\beta$  experiments do not observe a signal despite reaching sensitivities  $|\langle m_{ee} \rangle| \lesssim 1$  meV, JUNO’s improved oscillation parameters would enable a much sharper determination of the Majorana CP phases under the assumption of complete cancellation.

## 5. Conclusion

In this paper, we have investigated the impact of the JUNO first data release on the  $0\nu 2\beta$  decay effective mass and the determination of Majorana CP phases. The improved precision on the oscillation parameters, particularly almost a factor of 25.9% reduction in the uncertainty of  $\sin^2 \theta_s$  and 37.3% reduction in  $\Delta m_s^2$  at  $3\sigma$  range, directly translates into 22% (23%) reduction in the uncertainty of the minimum effective Majorana mass for IO (NO). At the  $3\sigma$  confidence level, we find  $\langle m_{ee} \rangle_{\min}^{\text{IO}} = (16.36 \sim 21.48)$  meV, with the narrowed range providing a more precise target for the next-generation  $0\nu\beta\beta$  experiments. This improvement is crucial for the experimental design of facilities such as nEXO, LEGEND-1000, and CUPID, which aim to probe the IO parameter space. The sharpened lower bound means that a null result from these experiments, combined with JUNO’s precision measurements, would provide increasingly strong evidence against the IO scenario. Nevertheless, the JUNO experiment can provide direct measurement of the neutrino mass ordering.

Beyond the bounds on  $\langle m_{ee} \rangle$ , the improved measurement of oscillation parameters at JUNO can also significantly enhance our ability to determine the Majorana CP phases  $\delta_{M1}$  and  $\delta_{M3}$  in the scenario of complete cancellation ( $\langle m_{ee} \rangle = 0$ ) for NO. For the narrow mass window  $m_1 = 3 \sim 6$  meV where a vanishing effective mass can exist, the allowed regions in the  $(\delta_{M1}, \delta_{M3})$  plane are substantially reduced from to previous analyses. Although simultaneous determination of the two Majorana CP phases is possible if future  $0\nu 2\beta$  experiments do not observe a signal when reaching the sensitivity of  $|\langle m_{ee} \rangle| \lesssim 1$  meV, it still relies on an experiment such as JUNO to reduce uncertainties from the particle physics side.

Looking ahead, the JUNO full dataset with several years of operation is expected to achieve sub-percent precision on  $\sin^2 \theta_s$ , which would further narrow the theoretical predictions for  $\langle m_{ee} \rangle$  in both mass orderings. This improvement will be especially valuable when combined with the next-generation  $0\nu 2\beta$  experiments as well as the absolute neutrino mass measurement from cosmological observations (such as DESI, EUCLID, and future CMB experiments) and beta decay experiments (such as PROJECT 8). The synergy of these three complementary measurements — the precision neutrino oscillation, the  $0\nu 2\beta$  decay, and the absolute mass scale determinations — forms an essential triad for fully characterizing the nature of neutrino masses. The results presented in this work demonstrate that the precision era of neutrino

physics has truly begun, with JUNO playing a central role in shaping the landscape of  $0\nu 2\beta$  decay phenomenology for the coming decade.

## Acknowledgements

The authors would like to thank Yue Meng for useful discussions. The authors are supported by the National Natural Science Foundation of China (12425506, 12375101, 12090060, and 12090064) and the SJTU Double First Class start-up fund (WF220442604). CFK is supported by IBS under the project code IBS-R018-D1. SFG is also an affiliate member of Kavli IPMU, University of Tokyo.

## References

- [1] A. G. Cohen, A. De Rújula, and S. L. Glashow, “*A matter-antimatter universe?*” *Astrophys. J.* **495** (1998) 539, [[arXiv:astro-ph/9707087](#)].
- [2] L. Canetti, M. Drewes, and M. Shaposhnikov, “*Matter and antimatter in the universe,*” *New J. Phys.* **14** (2012) 095012, [[arXiv:1204.4186](#)].
- [3] Alan H. Guth, “*Inflationary universe: A possible solution to the horizon and flatness problems,*” *Phys. Rev. D* **23** (1981) 347.
- [4] A. D. Sakharov, “*Violation of CP Invariance, C asymmetry, and baryon asymmetry of the universe,*” *Pisma Zh. Eksp. Teor. Fiz.* **5** (1967) 32–35.
- [5] M. Fukugita and T. Yanagida, “*Baryogenesis without grand unification,*” *Phys. Lett. B* **174** (1986) 45.
- [6] H. Fritzsch, Murray Gell-Mann, and P. Minkowski, “*Vector - Like Weak Currents and New Elementary Fermions,*” *Phys. Lett. B* **59** (1975) 256–260.
- [7] Peter Minkowski, “ *$\mu \rightarrow e\gamma$  at a Rate of One Out of  $10^9$  Muon Decays?,*” *Phys. Lett. B* **67** (1977) 421–428.
- [8] Tsutomu Yanagida, “*Horizontal gauge symmetry and masses of neutrinos,*” *Conf. Proc. C* **7902131** (1979) 95–99.
- [9] Murray Gell-Mann, Pierre Ramond, and Richard Slansky, “*Complex Spinors and Unified Theories,*” *Conf. Proc. C* **790927** (1979) 315–321, [[arXiv:1306.4669](#) [hep-th]].
- [10] S. L. Glashow, “*The Future of Elementary Particle Physics,*” *NATO Sci. Ser. B* **61** (1980) 687.
- [11] Rabindra N. Mohapatra and Goran Senjanovic, “*Neutrino Mass and Spontaneous Parity Nonconservation,*” *Phys. Rev. Lett.* **44** (1980) 912.

- [12] W. Konetschny and W. Kummer, “*Nonconservation of Total Lepton Number with Scalar Bosons*,” [Phys. Lett. B \*\*70\*\* \(1977\) 433–435](#).
- [13] M. Magg and C. Wetterich, “*Neutrino Mass Problem and Gauge Hierarchy*,” [Phys. Lett. B \*\*94\*\* \(1980\) 61–64](#).
- [14] J. Schechter and J. W. F. Valle, “*Neutrino Decay and Spontaneous Violation of Lepton Number*,” [Phys. Rev. D \*\*25\*\* \(1982\) 774](#).
- [15] T. P. Cheng and Ling-Fong Li, “*Neutrino Masses, Mixings and Oscillations in  $SU(2) \times U(1)$  Models of Electroweak Interactions*,” [Phys. Rev. D \*\*22\*\* \(1980\) 2860](#).
- [16] George Lazarides, Q. Shafi, and C. Wetterich, “*Proton Lifetime and Fermion Masses in an  $SO(10)$  Model*,” [Nucl. Phys. B \*\*181\*\* \(1981\) 287–300](#).
- [17] Rabindra N. Mohapatra and Goran Senjanovic, “*Neutrino Masses and Mixings in Gauge Models with Spontaneous Parity Violation*,” [Phys. Rev. D \*\*23\*\* \(1981\) 165](#).
- [18] Robert Foot, H. Lew, X. G. He, and Girish C. Joshi, “*Seesaw Neutrino Masses Induced by a Triplet of Leptons*,” [Z. Phys. C \*\*44\*\* \(1989\) 441](#).
- [19] Ernest Ma, “*Pathways to naturally small neutrino masses*,” [Phys. Rev. Lett. \*\*81\*\* \(1998\) 1171–1174](#), [[arXiv:hep-ph/9805219](#)].
- [20] Jeff A. Dror, Takashi Hiramatsu, Kazunori Kohri, Hitoshi Murayama, and Graham White, “*Testing the Seesaw Mechanism and Leptogenesis with Gravitational Waves*,” [Phys. Rev. Lett. \*\*124\*\* no. 4, \(2020\) 041804](#), [[arXiv:1908.03227](#) [hep-ph]].
- [21] Yanou Cui and Zhong-Zhi Xianyu, “*Probing Leptogenesis with the Cosmological Collider*,” [Phys. Rev. Lett. \*\*129\*\* no. 11, \(2022\) 111301](#), [[arXiv:2112.10793](#) [hep-ph]].
- [22] Michelle J. Dolinski, Alan W. P. Poon, and Werner Rodejohann, “*Neutrinoless Double-Beta Decay: Status and Prospects*,” [Ann. Rev. Nucl. Part. Sci. \*\*69\*\* \(2019\) 219–251](#), [[arXiv:1902.04097](#) [nucl-ex]].
- [23] Jack D. Shergold, “*Updated detection prospects for relic neutrinos using coherent scattering*,” [JCAP \*\*11\*\* no. 11, \(2021\) 052](#), [[arXiv:2109.07482](#) [hep-ph]].
- [24] Matteo Agostini, Giovanni Benato, Jason A. Detwiler, Javier Menéndez, and Francesco Vissani, “*Toward the discovery of matter creation with neutrinoless  $\beta\beta$  decay*,” [Rev. Mod. Phys. \*\*95\*\* no. 2, \(2023\) 025002](#), [[arXiv:2202.01787](#) [hep-ex]].
- [25] Vincenzo Cirigliano et al., “*Neutrinoless Double-Beta Decay: A Roadmap for Matching Theory to Experiment*,” [[arXiv:2203.12169](#) [hep-ph]].
- [26] J. Schechter and J. W. F. Valle, “*Neutrinoless double- $\beta$  decay in  $su(2) \times u(1)$  theories*,” [Phys. Rev. D \*\*25\*\* \(1982\) 2951](#).
- [27] J. Kotila and F. Iachello, “*Phase space factors for double- $\beta$  decay*,” [Phys. Rev. C \*\*85\*\* \(2012\) 034316](#), [[arXiv:1209.5722](#) [nucl-th]].

- [28] J. Kotila and F. Iachello, “Phase space factors for  $\beta^+\beta^+$  decay and competing modes of double- $\beta$  decay,” *Phys. Rev. C* **87** no. 2, (2013) 024313, [[arXiv:1303.4124](#) [nucl-th]].
- [29] M. Mirea, T. Pahomi, and S. Stoica, “Phase Space Factors for Double Beta Decay: an up-date,” [[arXiv:1411.5506](#) [nucl-th]].
- [30] Andrei Neacsu and Mihai Horoi, “An effective method to accurately calculate the phase space factors for  $\beta^-\beta^-$  decay,” *Adv. High Energy Phys.* **2016** (2016) 7486712, [[arXiv:1510.00882](#) [nucl-th]].
- [31] M. T. Mustonen and J. Engel, “Large-scale calculations of the double- $\beta$  decay of  $^{76}\text{Ge}$ ,  $^{130}\text{Te}$ ,  $^{136}\text{Xe}$ , and  $^{150}\text{Nd}$  in the deformed self-consistent skyrme quasiparticle random-phase approximation,” *Phys. Rev. C* **87** (2013) 064302.
- [32] J. Hyvarinen and J. Suhonen, “Nuclear matrix elements for  $0\nu\beta\beta$  decays with light or heavy majorana-neutrino exchange,” *Phys. Rev. C* **91** (2015) 024613.
- [33] F. Šimkovic, R. Dvornický, Dušan Stefánik, and A. Faessler, “Improved description of the  $2\nu\beta\beta$ -decay and a possibility to determine the effective axial-vector coupling constant,” *Phys. Rev. C* **97** (2018) 034315.
- [34] D.-L. Fang, A. Faessler, and F. Šimkovic, “ $0\nu\beta\beta$ -decay nuclear matrix element for light and heavy neutrino mass mechanisms from deformed quasiparticle random-phase approximation calculations for  $^{76}\text{Ge}$ ,  $^{82}\text{Se}$ ,  $^{130}\text{Te}$ ,  $^{136}\text{Xe}$ , and  $^{150}\text{Nd}$  with isospin restoration,” *Phys. Rev. C* **97** (2018) 045503.
- [35] J. Terasaki, “Strength of the isoscalar pairing interaction determined by a relation between double-charge change and double-pair transfer for double- $\beta$  decay,” *Phys. Rev. C* **102** no. 4, (2020) 044303, [[arXiv:2003.03542](#) [nucl-th]].
- [36] J. Menéndez, “Neutrinoless  $\beta\beta$  decay mediated by the exchange of light and heavy neutrinos: The role of nuclear structure correlations,” *J. Phys. G* **45** (2018) 014003.
- [37] M. Horoi and A. Neacsu, “Shell model predictions for  $^{124}\text{Sn}$  double- $\beta$  decay,” *Phys. Rev. C* **93** (2016) 024308.
- [38] L. Coraggio, A. Gargano, N. Itaco, R. Mancino, and F. Nowacki, “The calculation of the neutrinoless double-beta decay matrix element within the realistic shell model,” *Phys. Rev. C* **101** (2020) 044315, [[arXiv:2001.00890](#)].
- [39] L. Coraggio, N. Itaco, G. De Gregorio, A. Gargano, R. Mancino, and F. Nowacki, “Shell-model calculation of  $^{100}\text{Mo}$  double- $\beta$  decay,” *Phys. Rev. C* **105** (2022) 034312.
- [40] T. R. Rodriguez and G. Martinez-Pinedo, “Energy density functional study of nuclear matrix elements for neutrinoless  $\beta\beta$  decay,” *Phys. Rev. Lett.* **105** (2010) 252503.
- [41] N. López Vaquero, T. R. Rodríguez, and J. L. Egido, “Shape and pairing fluctuations effects on neutrinoless double beta decay nuclear matrix elements,” *Phys. Rev. Lett.* **111** (2013) 142501.

- [42] L. S. Song, J. M. Yao, P. Ring, and J. Meng, “*Nuclear matrix element of neutrinoless double- $\beta$  decay: Relativity and short-range correlations*,” *Phys. Rev. C* **95** (2017) 024305.
- [43] J. Barea, J. Kotila, and F. Iachello, “ *$0\nu\beta\beta$  and  $2\nu\beta\beta$  nuclear matrix elements in the interacting boson model with isospin restoration*,” *Phys. Rev. C* **91** (2015) 034304.
- [44] F. F. Deppisch, L. Graf, F. Iachello, and J. Kotila, “*Analysis of light neutrino exchange and short-range mechanisms in  $0\nu\beta\beta$  decay*,” *Phys. Rev. D* **102** no. 9, (2020) 095016, [[arXiv:2009.10119](#) [hep-ph]].
- [45] J. Carlson, S. Gandolfi, F. Pederiva, S. C. Pieper, R. Schiavilla, K. E. Schmidt, and R. B. Wiringa, “*Quantum monte carlo methods for nuclear physics*,” *Rev. Mod. Phys.* **87** (2015) 1067–1118.
- [46] B. R. Barrett, P. Navrátil, and J. P. Vary, “*Ab initio no core shell model*,” *Prog. Part. Nucl. Phys.* **69** (2013) 131–181.
- [47] P. Navrátil, S. Quaglioni, G. Hupin, C. Romero-Redondo, and A. Calci, “*Unified ab initio approaches to nuclear structure and reactions*,” *Phys. Scripta* **91** (2016) 053002.
- [48] K. Hebeler, J. D. Holt, J. Menendez, and A. Schwenk, “*Nuclear forces and their impact on neutron-rich nuclei and neutron-rich matter*,” *Ann. Rev. Nucl. Part. Sci.* **65** (2015) 457–484.
- [49] H. Hergert, S. K. Bogner, T. D. Morris, A. Schwenk, and K. Tsukiyama, “*The in-medium similarity renormalization group: A novel ab initio method for nuclei*,” *Phys. Rept.* **621** (2016) 165–222.
- [50] G. Hagen, T. Papenbrock, M. Hjorth-Jensen, and D. J. Dean, “*Coupled-cluster computations of atomic nuclei*,” *Rept. Prog. Phys.* **77** (2014) 096302.
- [51] M. Freer, H. Horiuchi, Y. Kanada-En’yo, D. Lee, and U.-G. Meißner, “*Microscopic clustering in light nuclei*,” *Rev. Mod. Phys.* **90** (2018) 035004.
- [52] S. Pascoli, S. T. Petcov, and T. Schwetz, “*The Absolute neutrino mass scale, neutrino mass spectrum, majorana CP-violation and neutrinoless double-beta decay*,” *Nucl. Phys. B* **734** (2006) 24–49, [[arXiv:hep-ph/0505226](#)].
- [53] Sandhya Choubey and Werner Rodejohann, “*Neutrinoless double beta decay and future neutrino oscillation precision experiments*,” *Phys. Rev. D* **72** (2005) 033016, [[arXiv:hep-ph/0506102](#)].
- [54] Manfred Lindner, Alexander Merle, and Werner Rodejohann, “*Improved limit on  $\theta(13)$  and implications for neutrino masses in neutrino-less double beta decay and cosmology*,” *Phys. Rev. D* **73** (2006) 053005, [[arXiv:hep-ph/0512143](#)].
- [55] Alexander Dueck, Werner Rodejohann, and Kai Zuber, “*Neutrinoless Double Beta Decay, the Inverted Hierarchy and Precision Determination of  $\theta(12)$* ,” *Phys. Rev. D* **83** (2011) 113010, [[arXiv:1103.4152](#) [hep-ph]].

- [56] Shao-Feng Ge and Werner Rodejohann, “*JUNO and Neutrinoless Double Beta Decay*,” *Phys. Rev. D* **92** no. 9, (2015) 093006, [[arXiv:1507.05514](#) [hep-ph]].
- [57] Shao-Feng Ge and Manfred Lindner, “*Extracting Majorana properties from strong bounds on neutrinoless double beta decay*,” *Phys. Rev. D* **95** no. 3, (2017) , [[arXiv:1608.01618](#) [hep-ph]].
- [58] Shao-Feng Ge and Jing-yu Zhu, “*Phenomenological Advantages of the Normal Neutrino Mass Ordering*,” *Chin. Phys. C* **44** no. 8, (2020) 083103, [[arXiv:1910.02666](#) [hep-ph]].
- [59] Shao-Feng Ge, Kaoru Hagiwara, Naotoshi Okamura, and Yoshitaro Takaesu, “*Determination of mass hierarchy with medium baseline reactor neutrino experiments*,” *JHEP* **05** (2013) 131, [[arXiv:1210.8141](#) [hep-ph]].
- [60] **JUNO** Collaboration, Fengpeng An et al., “*Neutrino Physics with JUNO*,” *J. Phys. G* **43** no. 3, (2016) 030401, [[arXiv:1507.05613](#) [physics.ins-det]].
- [61] Ivan Esteban, M. C. Gonzalez-Garcia, Michele Maltoni, Ivan Martinez-Soler, João Paulo Pinheiro, and Thomas Schwetz, “*NuFit-6.0: updated global analysis of three-flavor neutrino oscillations*,” *JHEP* **12** (2024) 216, [[arXiv:2410.05380](#) [hep-ph]].
- [62] **JUNO** Collaboration, Angel Abusleme et al., “*First measurement of reactor neutrino oscillations at JUNO*,” [[arXiv:2511.14593](#) [hep-ex]].
- [63] **KATRIN** Collaboration, M. Aker et al., “*Direct neutrino-mass measurement with sub-electronvolt sensitivity*,” *Nature Phys.* **18** (2022) 160–166, [[arXiv:2105.08533](#) [hep-ex]].
- [64] **KATRIN** Collaboration, M. Aker et al., “*KATRIN: Status and Prospects for the Neutrino Mass and Beyond*,” *J. Phys. G* **51** no. 10, (6, 2024) 103001, [[arXiv:2406.13516](#) [hep-ex]].
- [65] **DESI** Collaboration, A. G. Adame et al., “*DESI 2024 VI: Cosmological Constraints from the Measurements of Baryon Acoustic Oscillations*,” *Astrophys. J.* **977** (4, 2024) 62, [[arXiv:2404.03002](#) [astro-ph.CO]].
- [66] **DESI** Collaboration, A. G. Adame et al., “*DESI 2024 III: Baryon Acoustic Oscillations from Galaxies and Quasars*,” *Astrophys. J.* **977** (4, 2024) 67, [[arXiv:2404.03000](#) [astro-ph.CO]].
- [67] **Planck** Collaboration, N. Aghanim et al., “*Planck 2018 results. VI. Cosmological parameters*,” *Astron. Astrophys.* **641** (2020) A6, [[arXiv:1807.06209](#) [astro-ph.CO]]. [Erratum: *Astron. Astrophys.* 652, C4 (2021)].
- [68] **Particle Data Group** Collaboration, S. Navas et al., “*Review of particle physics*,” *Phys. Rev. D* **110** no. 3, (2024) 030001.
- [69] Francesco Vissani, “*Signal of neutrinoless double beta decay, neutrino spectrum and oscillation scenarios*,” *JHEP* **06** (1999) 022, [[arXiv:hep-ph/9906525](#)].

- [70] Zhi-zhong Xing and Ye-Ling Zhou, “*Geometry of the effective Majorana neutrino mass in the  $0\nu\beta\beta$  decay*,” *Chin. Phys. C* **39** (2015) 011001, [[arXiv:1404.7001](#) [hep-ph]].
- [71] S. Pascoli and S. T. Petcov, “*The SNO solar neutrino data, neutrinoless double beta decay and neutrino mass spectrum*,” *Phys. Lett. B* **544** (2002) 239–250, [[arXiv:hep-ph/0205022](#)].
- [72] F. T. Avignone, G. S. King, and Yu. G. Zdesenko, “*Next generation double-beta decay experiments: Metrics for their evaluation*,” *New J. Phys.* **7** (2005) 6.
- [73] **KamLAND-Zen** Collaboration, S. Abe et al., “*Search for Majorana Neutrinos with the Complete KamLAND-Zen Dataset*,” [[arXiv:2406.11438](#) [hep-ex]].
- [74] **KamLAND-Zen** Collaboration, S. Abe et al., “*Search for the Majorana Nature of Neutrinos in the Inverted Mass Ordering Region with KamLAND-Zen*,” *Phys. Rev. Lett.* **130** no. 5, (2023) 051801, [[arXiv:2203.02139](#) [hep-ex]].
- [75] **nEXO** Collaboration, J. B. Albert et al., “*Sensitivity and Discovery Potential of nEXO to Neutrinoless Double Beta Decay*,” *Phys. Rev. C* **97** no. 6, (2018) 065503, [[arXiv:1710.05075](#) [nucl-ex]].
- [76] **nEXO** Collaboration, G Adhikari et al., “*nEXO: neutrinoless double beta decay search beyond  $10^{28}$  year half-life sensitivity*,” *J. Phys. G* **49** no. 1, (2022) 015104, [[arXiv:2106.16243](#) [nucl-ex]].
- [77] **LEGEND** Collaboration, N. Abgrall et al., “*The Large Enriched Germanium Experiment for Neutrinoless  $\beta\beta$  Decay: LEGEND-1000 Preconceptual Design Report*,” *J. Phys. G* **49** no. 1, (2022) 015104, [[arXiv:2107.11462](#) [physics.ins-det]].
- [78] **LEGEND** Collaboration, N. Abgrall et al., “*The Large Enriched Germanium Experiment for Neutrinoless Double Beta Decay: LEGEND-1000 Preconceptual Design Report*,” *J. Phys. G* **49** no. 1, (2022) 015104, [[arXiv:2107.11462](#) [physics.ins-det]].
- [79] **CUPID** Collaboration, K. Alfonso et al., “*CUPID pre-CDR*,” *J. Low Temp. Phys.* **211** (2023) 375–383, [[arXiv:2203.08386](#) [physics.ins-det]].
- [80] **CUPID** Collaboration, E Armengaud et al., “*New Limit for Neutrinoless Double-Beta Decay of  $^{100}\text{Mo}$  from the CUPID-Mo Experiment*,” *Phys. Rev. Lett.* **126** no. 18, (2021) 181802, [[arXiv:2011.13243](#) [nucl-ex]].
- [81] **KamLAND-Zen** Collaboration, A. Gando et al., “*Search for Majorana Neutrinos near the Inverted Mass Hierarchy Region with KamLAND-Zen*,” *Phys. Rev. Lett.* **117** no. 8, (2016) 082503, [[arXiv:1605.02889](#) [hep-ex]]. Erratum: *Phys. Rev. Lett.* **117**, 109903 (2016).
- [82] M. Agostini et al., “*Background-free search for neutrinoless double- $\beta$  decay of  $^{76}\text{Ge}$  with GERDA*,” *Nature* **544** (2017) 47, [[arXiv:1703.00570](#) [nucl-ex]].

- [83] **Majorana** Collaboration, I. J. Arnquist et al., “*Final Result of the Majorana Demonstrator’s Search for Neutrinoless Double- $\beta$  Decay in Ge76*,” *Phys. Rev. Lett.* **130** no. 6, (2023) 062501, [[arXiv:2207.07638](#) [nucl-ex]].
- [84] **EXO-200** Collaboration, G. Anton et al., “*Search for Neutrinoless Double- $\beta$  Decay with the Complete EXO-200 Dataset*,” *Phys. Rev. Lett.* **123** no. 16, (2019) 161802, [[arXiv:1906.02723](#) [hep-ex]].
- [85] **CUORE** Collaboration, D. Q. Adams et al., “*Improved Limit on Neutrinoless Double-Beta Decay in  $^{130}\text{Te}$  with CUORE*,” *Nature* **604** (2022) 53–58, [[arXiv:2104.06906](#) [nucl-ex]].
- [86] **CUPID** Collaboration, K. Alfonso et al., “*CUPID pre-CDR*,” *J. Low Temp. Phys.* **211** (2023) 375–383.
- [87] **DARWIN** Collaboration, F. Agostini et al., “*Sensitivity of the DARWIN observatory to the neutrinoless double beta decay of  $^{136}\text{Xe}$* ,” *Eur. Phys. J. C* **80** no. 9, (2020) 808, [[arXiv:2003.13407](#) [physics.ins-det]].
- [88] **KamLAND-Zen** Collaboration, S. Abe et al., “*Search for the Majorana Nature of Neutrinos in the Inverted Mass Ordering Region with KamLAND-Zen*,” *Phys. Rev. Lett.* **130** no. 5, (2023) 051801, [[arXiv:2203.02139](#) [hep-ex]].
- [89] **NEXT** Collaboration, C. Adams et al., “*Sensitivity of a tonne-scale NEXT detector for neutrinoless double beta decay searches*,” *JHEP* **2021** no. 08, (2021) 164, [[arXiv:2005.06467](#) [physics.ins-det]].
- [90] **SNO+** Collaboration, V. Albanese et al., “*The SNO+ experiment*,” *JINST* **16** no. 08, (2021) P08059, [[arXiv:2104.11687](#) [physics.ins-det]].
- [91] **AMoRE** Collaboration, M. H. Lee, “*AMoRE: A search for neutrinoless double-beta decay of  $^{100}\text{Mo}$  using low-temperature molybdenum-containing crystal detectors*,” *JINST* **15** no. 08, (2020) C08010, [[arXiv:2005.05567](#) [physics.ins-det]].
- [92] **SuperNEMO** Collaboration, R. Arnold, C. Augier, J. D. Baker, A. S. Barabash, A. Basharina-Freshville, et al., “*Probing New Physics Models of Neutrinoless Double Beta Decay with SuperNEMO*,” *Eur. Phys. J. C* **70** (2010) 927–943, [[arXiv:1005.1241](#) [hep-ex]].
- [93] Euclid Collaboration, “*Euclid preparation: VII. Forecast validation for Euclid cosmological probes*,” *Astron. Astrophys.* **642** (2020) A191, [[arXiv:1910.09273](#) [astro-ph.CO]].
- [94] Euclid Collaboration, “*Euclid preparation: XV. Forecasting cosmological constraints for the Euclid and CMB joint analysis*,” *Astron. Astrophys.* **666** (2022) A200, [[arXiv:2206.14067](#) [astro-ph.CO]].

- [95] Sunny Vagnozzi, Elena Giusarma, Olga Mena, Katherine Freese, Martina Gerbino, Shirley Ho, and Massimiliano Lattanzi, “*Unveiling  $\nu$  secrets with cosmological data: neutrino masses and mass hierarchy*,” *Phys. Rev. D* **96** no. 12, (2017) 123503, [[arXiv:1701.08172](#) [astro-ph.CO]].
- [96] Stefano Gariazzo et al., “*Neutrino mass and mass ordering: no conclusive evidence for normal ordering*,” *JCAP* **10** (2022) 010, [[arXiv:2205.02195](#) [hep-ph]].
- [97] Eleonora Di Valentino et al., “*Cosmology Intertwined III:  $f\sigma_8$  and  $S_8$* ,” *Astropart. Phys.* **131** (2021) 102604, [[arXiv:2008.11285](#) [astro-ph.CO]].
- [98] Christiane S. Lorenz, Erminia Calabrese, and David Alonso, “*Distinguishing between Neutrinos and time-varying Dark Energy through Cosmic Time*,” *Phys. Rev. D* **96** no. 4, (2017) 043510, [[arXiv:1706.00730](#) [astro-ph.CO]].
- [99] Maria Archidiacono, Deanna C. Hooper, Riccardo Murgia, Sebastian Bohr, Julien Lesgourgues, and Matteo Viel, “*Constraining Dark Matter-Dark Radiation interactions with CMB, BAO, and Lyman- $\alpha$* ,” *JCAP* **10** (2019) 055, [[arXiv:1907.01496](#) [astro-ph.CO]].
- [100] Shouvik Roy Choudhury and Steen Hannestad, “*Updated results on neutrino mass and mass hierarchy from cosmology with Planck 2018 likelihoods*,” *JCAP* **07** (2020) 037, [[arXiv:1907.12598](#) [astro-ph.CO]].
- [101] Francesco Forastieri, Massimiliano Lattanzi, and Paolo Natoli, “*Cosmological constraints on neutrino self-interactions with a light mediator*,” *Phys. Rev. D* **100** no. 10, (2019) 103526, [[arXiv:1904.07810](#) [astro-ph.CO]].
- [102] Mathias Garny, Thomas Konstandin, Laura Sagunski, and Matteo Viel, “*Neutrino mass bounds from confronting an effective model with BOSS Lyman- $\alpha$  data*,” *JCAP* **03** (2021) 049, [[arXiv:2011.03050](#) [astro-ph.CO]].
- [103] Shao-Feng Ge, Pedro Pasquini, and Liang Tan, “*Neutrino mass measurement with cosmic gravitational focusing*,” *JCAP* **05** (2024) 108, [[arXiv:2312.16972](#) [hep-ph]].
- [104] Shao-Feng Ge and Liang Tan, “*Identifying neutrino mass ordering with cosmic gravitational focusing*,” *Phys. Rev. D* **111** no. 8, (2025) 083539, [[arXiv:2409.11115](#) [hep-ph]].
- [105] **KATRIN** Collaboration, M. Aker et al., “*Improved Upper Limit on the Neutrino Mass from a Direct Kinematic Method by KATRIN*,” *Phys. Rev. Lett.* **123** (2019) 221802, [[arXiv:1909.06048](#) [hep-ex]].
- [106] **Project 8** Collaboration, D. M. Asner et al., “*Single electron detection and spectroscopy via relativistic cyclotron radiation*,” *Phys. Rev. Lett.* **114** (2015) 162501, [[arXiv:1408.5362](#) [physics.ins-det]].

- [107] **Project 8** Collaboration, A. Ashtari Esfahani et al., “*Determining the neutrino mass with cyclotron radiation emission spectroscopy—Project 8*,” *J. Phys. G* **44** (2017) 054004, [[arXiv:1703.02037](#) [physics.ins-det]].
- [108] Andreas Ringwald, “*Prospects for the direct detection of the cosmic neutrino background*,” *Nucl. Phys. A* **827** (2009) 501C–506C, [[arXiv:0901.1529](#) [astro-ph.CO]].
- [109] Petr Vogel, “*How difficult it would be to detect cosmic neutrino background?*,” *AIP Conf. Proc.* **1666** no. 1, (2015) 140003.
- [110] D. N. Dinh, S. T. Petcov, N. Sasao, M. Tanaka, and M. Yoshimura, “*Observables in Neutrino Mass Spectroscopy Using Atoms*,” *Phys. Lett. B* **719** (2013) 154–163, [[arXiv:1209.4808](#) [hep-ph]].
- [111] Atsushi Fukumi et al., “*Neutrino Spectroscopy with Atoms and Molecules*,” *PTEP* **2012** (2012) 04D002, [[arXiv:1211.4904](#) [hep-ph]].